atmosphere

MDPI

Article

Study on Wind Simulations Using Deep Learning Techniques during Typhoons: A Case Study of Northern Taiwan

Chih-Chiang Wei

Department of Marine Environmental Informatics & Center of Excellence for Ocean Engineering, National Taiwan Ocean University, No.2, Beining Rd., Jhongjheng District, Keelung City 20224, Taiwan; ccwei@ntou.edu.tw; Tel.: +886-2-24622192

Received: 28 July 2019; Accepted: 5 November 2019; Published: 7 November 2019

Abstract: A scheme for wind-speed simulation during typhoons in Taiwan is highly desirable, considering the effects of the powerful winds accompanying the severe typhoons. The developed combination of deep learning (DL) algorithms with a weather-forecasting numerical model can be used to determine wind speed in a rapid simulation process. Here, the Weather Research and Forecasting (WRF) numerical model was employed as the numerical simulation-based model for precomputing solutions to determine the wind velocity at arbitrary positions where the wind cannot be measured. The deep neural network (DNN) was used for constructing the DL-based wind-velocity simulation model. The experimental area of Northern Taiwan was used for the simulation. Regarding the complex typhoon system, the collected data comprised the typhoon tracks, FNL (Final) Operational Global Analysis Data for the WRF model, typhoon characteristics, and ground weather data. This study included 47 typhoon events that occurred over 2000–2017. Three measures were used to analyze the models for identifying optimal performance levels: Mean absolute error, root mean squared error, and correlation coefficient. This study compared observations with the WRF numerical model and DNN model. The results revealed that (1) simulations by using the WRF-based models were satisfactorily consistent with the observed data and (2) simulations by using the DNN model were considerably consistent with those of the WRF-based model. Consequently, the proposed DNN combined with WRF model can be effectively used in simulations of wind velocity at arbitrary positions of study area.

Keywords: wind speed; deep neural networks; numerical model; typhoon; performance evaluation

1. Introduction

Typhoons are primarily generated in the intertropical convergence zone on the western side of the Pacific Ocean and are affected by high-level subtropical peripheral airflow of the subtropical high, mostly moving toward the west or Northwest. Taiwan (21°54′ N–25°18′ N, 120° E–122° E) has a subtropical climate and is on the main path of typhoons in the Western Pacific region (Figure 1). Historically, an average of 3–4 typhoons per year pass near or over Taiwan. Strong typhoon winds blow over the sea and land and produce large waves with energy sufficient to influence marine structures and erode beaches and buildings [1]. Therefore, because of the effects of these powerful winds accompanying these severe typhoons, a reliable and efficient scheme for wind speed simulations during typhoons in Taiwan is highly desirable.

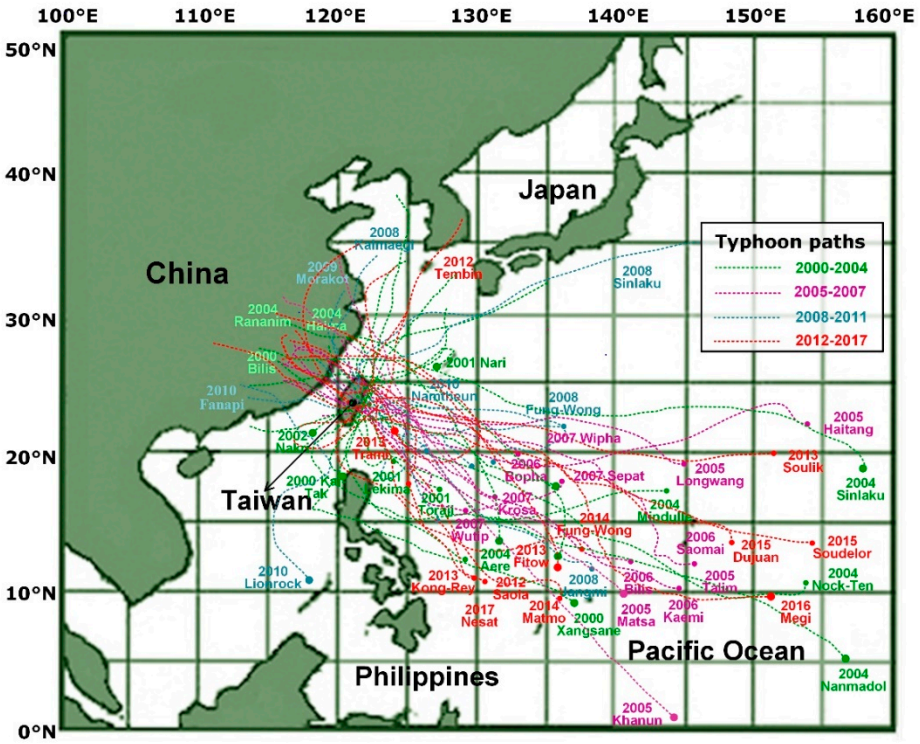

Figure 1. Location of Taiwan and historical typhoon events that affected Taiwan.

The numerical weather prediction (NWP) model is a method of weather simulation that employs a set of equations that describe the flow of fluids. These equations are translated into computer code and use governing equations, numerical methods, parameterizations of other physical processes and combined with initial and boundary conditions before being run over a geographic area [2–5]. Numerous models have been developed to investigate weather-forecasting processes: For instance, Yang and Ching [6] investigated the dependence of the simulated track, central pressure, maximum wind, and accumulated rainfall of Typhoon Toraji in 2001 on physical parameterizations. Moreover, Davis et al. [7] described the process of applying an object-based verification methodology to forecast rainfall during warm seasons in the continental United States.

The Weather Research and Forecasting (WRF) numerical model [8] is a commonly used, community mesoscale NWP model [9,10]. The WRF model offers two dynamic solvers for computing the atmospheric governing equations: Advanced Research WRF (ARW) solver and Nonhydrostatic Mesoscale Model. Numerous studies on the WRF numerical model with tropical cyclones have been conducted recently [11–16]. For instance, Tao et al. [17] indicated that WRF is able to capture the amount and location of the observed surface rainfall and that the typhoon-induced circulation, orographic lifting and a moisture-abundant southwest flow are the main mechanisms that together produced the tremendous rainfall. Xu et al. [18] conducted WRF model in simulating Typhoon Morakot over Taiwan. Hsiao et al. [19] developed an ensemble modeling system (WRF and the fifth-generation Pennsylvania State University–National Center for Atmospheric Research Mesoscale Model (MM5)) coupled with a hydrological model to predict typhoon rainfall and flood responses in a watershed in Taiwan. Wu et al. [20] determined the grid parameters of the WRF model in the simulation of Typhoon Kai-Tak.

In addition to the numerous physical models currently available, the development of the field of machine learning (ML) has also increased the frequency with which data-driven models, defined as computer programming in which program statements describe data to be matched and the processing required, are used [21–23]. The ML model and statistical methods are based on myriad historical data not considering the meteorological conditions. Data-driven models are generally accepted as a feasible approach for establishing the capability for wind-speed predictions [24–30]. For instance, Li et al. [31] proposed a data-driven model for determining the wind-power spectrum of a typhoon

according to analytical considerations and field measurements of typhoons in the South China Sea. Wei [32] developed a highly reliable surface wind-speed prediction technique, namely a kernel-based support vector machine for a regression model. Hu et al. [33] introduced deep neural networks (DNNs), trained using data from data-rich wind plants, to extract wind-speed patterns and then finely tune the mapping with the data from newly constructed wind plants. Moreover, a hybrid method by combining physical and statistical methods and using weather forecasts and time-series analysis has been proposed. For instance, Zhao et al. [5] presented the performance evaluation and accuracy enhancement of a day-ahead wind-power forecasting system, comprising a NWP model and artificial neural networks (ANNs).

This study developed a typhoon surface wind-speed simulation model by DL-based models using NWP numerical solutions. That is, it involves the development of a method for simulating surface wind speeds during typhoons by combining deep learning (DL) and NWP. DL is a specific subfield of ML intended to enable machines to simulate the way the human brain thinks, and its operational model is based on neuroscience [34–36]. The concept of DL originates from research on ANNs and alleviates the problem of local optima in the nonconvex objective function of deep networks. Three attributes—a larger number of hidden units (neurons) and superior learning algorithm and parameter initialization technique—have contributed to the success of the DL approach [33].

In general, the advantages of numerical models are rooted in the fact that all parameters are calculated through atmospheric dynamics and numerical methods. Therefore, the simulated results can be explained through physical relationships. In numerical models, data assimilation and objective analysis can provide the reasonable initial conditions for kinetics models. However, numerical model simulations often require a large amount of time for conducting calculations—from several hours to several days, based on the efficiency of the calculation processor and the scale of the calculation [37]. Generally, statistical models exhibit higher calculation efficiency than do numerical weather prediction because statistical models establish statistical relationships between target variables and other attributes based on data from observations recorded across a long period and then apply appropriate statistical methods to rapidly construct simulation models. However, for statistical models, the physical fundamentals are relatively weak. For instance, two parameters may have a strong statistical relationship, but no explainable physical cause-and-effect relationship. Alternatively, a clearly visible physical relationship between two parameters may not be reflected by statistical analysis. Therefore, statistical models exhibit limitations because they do not offer the insight into physical processes that is provided by full-scale numerical models. The concept of this study stems from the desire to establish an approach that combines the advantages of both models to generate simulations that are considerably prompt and accurate.

The remainder of this paper is organized as follows: Section 2 describes the description of the study area and data. Section 3 presents a methodology of DL combined with the NWP model. Section 4 provides the outcomes obtained from the NWP-based WRF numerical model. Sections 5 and 6 evaluations of DL-based DNN models using the WRF outcomes and comparisons of testing-typhoon simulations. Finally, Section 7 presents the conclusion.

2. Study Region and Data

This study used Northern Taiwan as the research area for wind-speed simulations (Figure 1), with two primary cities: Taipei and Keelung. The Taipei metropolitan area has a population of 7.04 million, whereas Keelung has a population of approximately 370 thousand. Northern Taiwan, located in an area over which major typhoons in the Northwestern Pacific Ocean may pass. To address essential typhoon precautions, improving wind-speed simulation capabilities in this area is essential.

This study collected data from 47 typhoon incidences (Table A1) that affected Northern Taiwan occurring over 2000–2017 and their paths (Figure 1). The data involved two types of data set: Typhoon characteristics and surface meteorological data, and comprised 8820 records measured at hourly intervals. The typhoon dynamics data can be obtained from a variety of information released by the

Central Weather Bureau (CWB) of Taiwan, including six attributes: pressure at the typhoon center, latitude of the typhoon center, longitude of the typhoon center, typhoon radius of the winds over 15.5 m/s, moving speed of the typhoon, and maximum wind speed of the typhoon center. In the paper, these attributes were encoded as T_k where k is the six typhoon dynamics attributes (k from 1 to 6).

Moreover, the meteorological data also released by the CWB include the hourly climatological characteristics. Surface meteorological data comprised six ground weather stations: Keelung, Penjiayu, Tamsui, Banqiao, Taipei, and Yilan (Figure 2). Each ground weather station collects data on the eight attributes. These climatological attributes were air pressure, temperature, dew-point temperature, relative humidity, vapor pressure, surface wind speed (10 m above the surface), surface wind direction, and precipitation. These attributes were encoded as $M_{i,j}$ where i is the ground weather stations (i from 1 to 6, for Keelung, Penjiayu, Tamsui, Banqiao, Taipei, and Yilan, respectively) and j represents eight climatological attributes (j from 1 to 8).

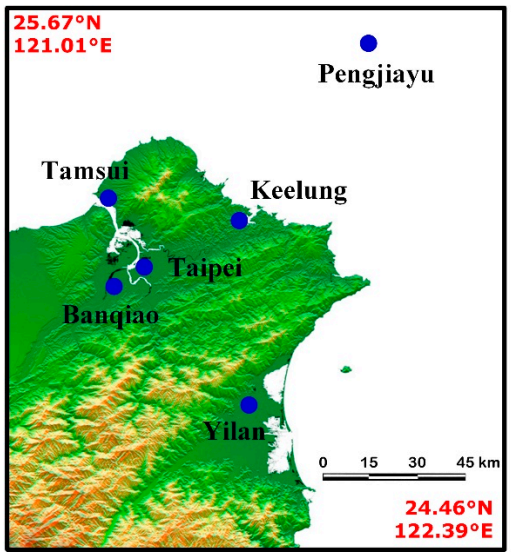

Figure 2. Map of Taiwan's northern region and meteorological stations.

3. Methodology

This study constructed a DL-based DNN wind-speed simulation model that can be applied in arbitrary points of study area. However, these arbitrary points lacked wind-speed observation data, that is, measures were absent. Therefore, the numerical solutions obtained from the WRF numerical model in the study were used to replace with observation data. Accordingly, we could capitalize on the ability of DL algorithmic models to rapidly conduct simulations and avoid long calculation time required for simulation in the NWP model.

Figure 3 illustrates the analysis flowchart for combining DL data-driven model with the NWP numerical model. In the figure, regarding the data preprocessing, the model constructed in this study used two types of data set: (1) typhoon characteristics and surface weather data, and (2) numerical simulation values provided by the WRF model. To verify the WRF-based wind-speed values is performed well enough to be used instead of observations, we compared the WRF model simulation values with the gauge-station observations. It is noted that when we formulated the WRF and the subsequent DL-based models, we selected weather stations managed by CWB as "arbitrary points" and used them for models verification purpose.

To evaluate simulation outcomes, this study adopted four criteria, namely mean absolute error (MAE), relative MAE (rMAE), root mean squared error (RMSE), relative RMSE (rRMSE), and correlation coefficient (r):

$$\mathrm{MAE} = \frac{1}{n}\sum_{i=1}^{n}|O_i - Y_i| \quad (1)$$

$$\text{rMAE} = \frac{\frac{1}{n}\sum_{i=1}^{n}|O_i - Y_i|}{\overline{O}} \tag{2}$$

$$\text{RMSE} = \sqrt{\frac{1}{n}\sum_{i=1}^{n}(O_i - Y_i)^2} \tag{3}$$

$$\text{rRMSE} = \frac{\sqrt{\frac{1}{n}\sum_{i=1}^{n}(O_i - Y_i)^2}}{\overline{O}} \tag{4}$$

$$\text{r} = \frac{\sum\left(Y_i - \overline{Y}\right)(O_i - \overline{O})}{\left[\sum\left(Y_i - \overline{Y}\right)^2 \sum\left(O_i - \overline{O}\right)^2\right]^{\frac{1}{2}}} \tag{5}$$

where Y_i is the estimated value of the record i, O_i the observation of the record i, $\overline{O}$ the mean of the observed values, $\overline{Y}$ the mean of the estimated values, and n the total number of records. MAE and RMSE represent absolute errors, whereas rMAE and rRMSE represent relative errors.

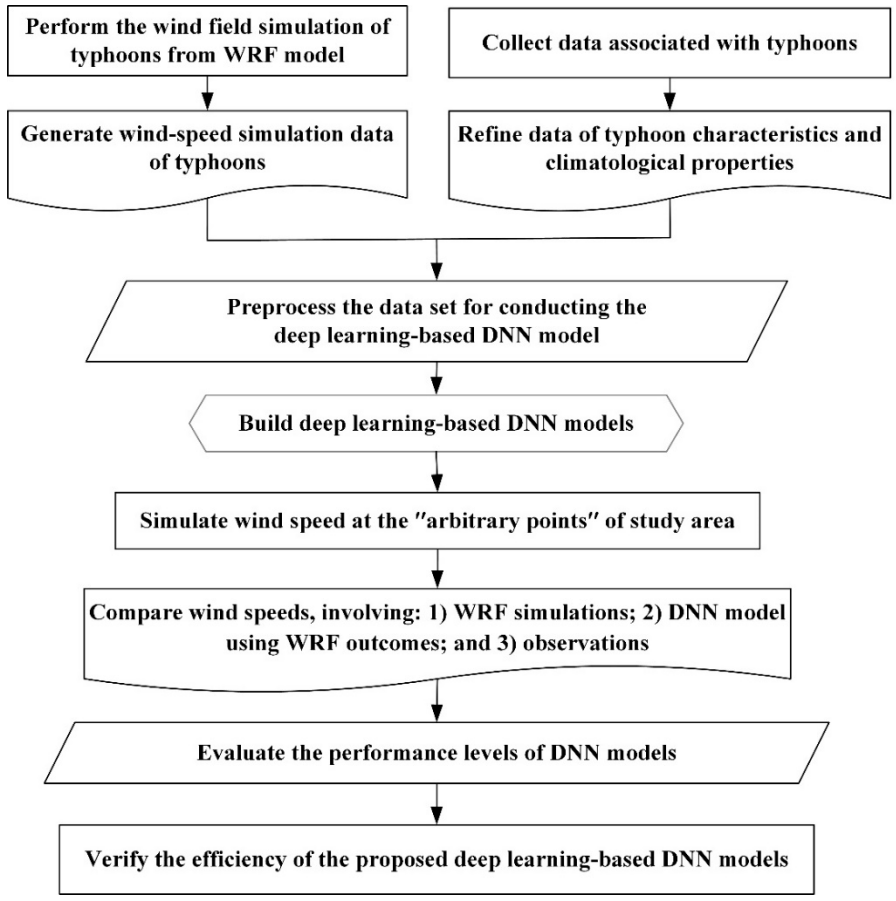

Figure 3. Flowchart of deep learning (DL)-based deep neural network (DNN) model combined with Weather Research and Forecasting (WRF) numerical model.

3.1. The WRF Model

The current WRF model version is 3.9; it has been available since 2017. This model offers multiple physics options that can be combined in different ways. The ARW is suitable for use in a broad range of applications across scales, ranging from meters to thousands of kilometers, and includes idealized simulations (e.g., large-eddy simulation, convection, and baroclinic waves), parameterization research, data assimilation research, forecast research, real-time NWP, hurricane research, regional

climate research, and coupled-model applications. Additional details can be found in the WRF Version 3 Modeling System User's Guide [38].

The model developed in the study was used to generate wind-speed simulations during typhoons. In the development of the model, this study first used the WRF numerical model to simulate the circulation distribution and wind-speed values at each grid point in the research area. The several typhoons were simulated to obtain the wind-speed values at each grid point in the area. In the process of modularization, the data on typhoons was collected from the U.S. National Center for Environmental Prediction (NCEP), and the Global Forecast System model analysis was used as the initial field for conducting numerical predictions for several consecutive days (depending on the length of the typhoon).

Figure 4 presents the flowchart of the WRF numerical model simulation. The simulation procedures included the following: Setting up the computation environment of WRF model; collecting historical typhoon data required for the model simulation process, and the initial field and boundary layer data; setting up the model parameters and simulation range; verifying and validating the model; outputting and processing simulation data; producing wind-field data for each typhoon; and post-processing a dataset preparing for the use of DL-based DNN models establishing.

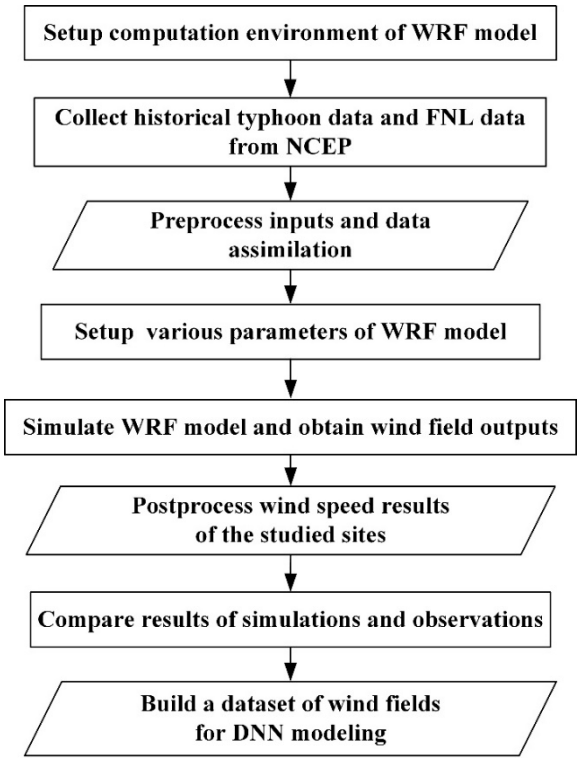

Figure 4. Conceptual flowchart of WRF model simulations. FNL—Final, NCEP—National Center for Environmental Prediction.

3.2. The DNN Model

The DNN is a feed-forward ANN with more than one layer of hidden units between its inputs and outputs [39]. Each hidden layer computes the activation of conditionally independent units with respect to the activations of the previous layer [40]. The activation functions are rules for mapping the sum of an individual weighted input to the output. By training the ANN processes, the optimal solutions for those weighted values are determined. Commonly adopted nonlinear activation functions are the sigmoid function, hyperbolic tangent function, and Gaussian function [36]. The rectified linear unit (ReLU) is an activation function defined as the positive part of its argument: $f(x) = \max(0, x)$,

where x is the input to a neuron. The ReLU function [41], which has become popular in recent years due to its simplicity and its ability to enable fast training [42].

The steps for the subsequent analysis include WRF simulations, building DL-based model using WRF simulation outcomes and outputting results from DL-based model. Then, we verify the results of DNN models according to the WRF simulations. Finally, we evaluate the performance levels of each model and compare the efficiency of these models.

4. WRF Model and Analysis

4.1. WRF Settings and Calculations

This study used the NCEP Global Data Assimilation System (GDAS) FNL (Final) Operational Global Analysis Data as the initial field and boundary conditions, including parameters such as sea-level pressure, sea-surface temperature, wind field, atmospheric temperature, surface temperature, soil cover, ice layer, and surface albedo. This study conducted WRF model simulations from 47 collected typhoons for several consecutive days for each typhoon for four daily numerical simulations for 12 h.

The start point for each simulation was 24 h before the CWB had issued a typhoon landing warning and the end point was 24 h after the warning had ended. In this study, the grid was set as a two-domain nested grid (Figure 5). The horizontal grid spacing for Domain 1 was 15 km (118° E–126° E, 21° N–29° N), whereas the horizontal grid spacing for Domain 2 was 5 km (121° E–123° E, 24° N–26° N). The vertical layering included 32 layers. Domain 1 was used to cover large-scale meteorological phenomena, such as typhoon movement paths, and Domain 2 was used to simulate medium to small-scale meteorological mesoscale alpha systems (200–2000 km scale), such as the effects of Taiwan's geography on typhoon circulation. The inner horizontal grid spacing of 5 km used in this study is suggested by [19] and [43–45].

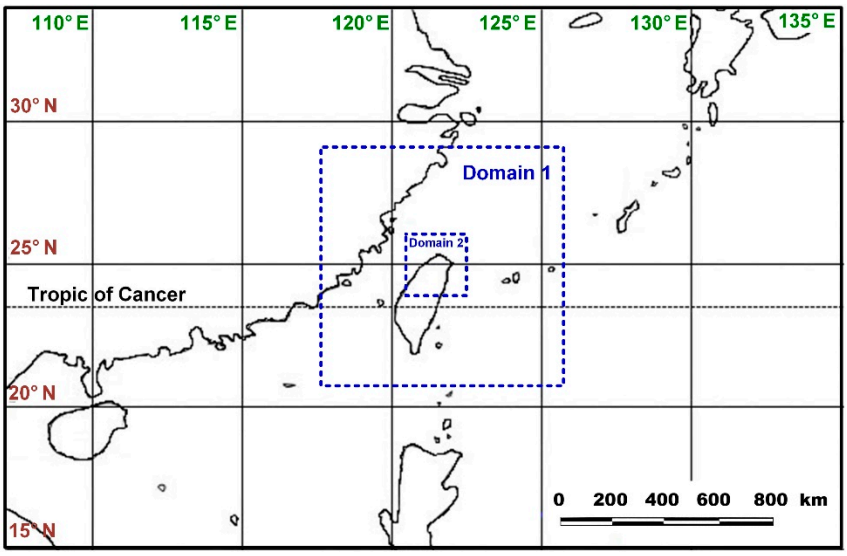

Figure 5. Area covered by two-layer nested grid: Domains 1 and 2.

The WRF model provides many types of physical parameter options enabling atmospheric research and use of operational units for different weather patterns, geographic areas, or conditions. To select a suitable parameter for a specific region (i.e., Taiwan), we referred Yeh et al. [43–45], a three-year project, regarding the studies on the typhoon track, rainfall and winds forecast using the WRF model over Taiwan. According their projects, they concluded that when typhoons strike Taiwan, the optimal physical parameter options are: planetary boundary layer = Yonsei University (YSU) scheme [46], parameter of microphysics = WRF Single-Moment 5-class (WSM5) scheme [47], the parameter of

cumulus parameterization = Kain–Fritsch scheme [48,49], and parameter of longwave radiation = Rapid Radiative Transfer Model (RRTM) scheme [50].

4.2. WRF Simulation Outcomes

After simulating numerous typhoon events using the WRF model, this study produced data from wind-field analysis for each *x*–*y* axis and *z* altitude typhoon event. Six primary ground weather stations were present in the study area: Taipei, Keelung, Pengjiayu, Tamsui, Banqiao, and Yilan stations. This study simulated the wind-speed values for the two stations of Taipei and Keelung. Because the ground gauge-station wind speed reached the observation value at an altitude of 10 m, the WRF model output objective was the simulated wind value at the same altitude to verify subsequent WRF wind outcomes.

This study performed a WRF model simulation of 47 typhoon events and obtained 4416 h of simulation values after organizing the outcomes. Figure 6 displays the scatter plot with all WRF model simulation values and observed ground station (Taipei and Keelung) values. The figure demonstrates that when the wind speed at Taipei and Keelung stations was greater than 9 m/s, the WRF model simulation values underestimated the wind speed. In terms of correlation, Taipei station (r = 0.7790) exhibited a greater overall correlation than did Keelung station (r = 0.7364). Because of the effects of the terrain, the observed wind speed at Keelung station ranged from 0 to 25 m/s, whereas those at Taipei station ranged from 0 to 15 m/s, indicating that the overall wind speed within the basin (Taipei station) was slower than that in the seaside areas (Keelung station). Furthermore, the slopes of the linear regression line (solid red line in Figure 6) for Taipei and Keelung stations were 0.5665 and 0.3955, respectively. Thus, the smaller slope for Keelung station indicated that the WRF model was more prone to underestimate the wind speed at Keeling station than at Taipei station.

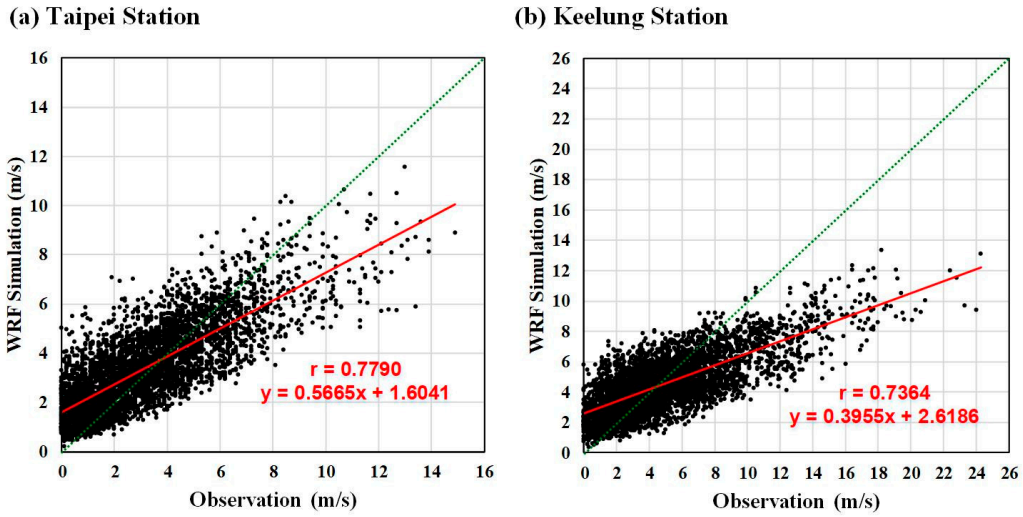

Figure 6. Scatterplots depicting observations vs WRF simulations: (**a**) Taipei station; (**b**) Keelung station.

Moreover, the results showed that the evaluation at Taipei station (MAE and rMAE = 1.142 m/s and 0.346, respectively) was superior to that at did Keelung station (1.865 m/s and 0.372, respectively); similarly, the evaluation at Taipei station (RMSE and rRMSE = 1.485 m/s and 0.449, respectively) was superior to that at Keelung station (2.498 m/s and 0.498, respectively). In general, the WRF simulations exhibited greater absolute and relative errors for Keelung station than for Taipei station.

5. DL Modeling using WRF Outcomes

In this section, this study used the DL-based DNN model to construct wind-speed simulation models for the Taipei and Keelung stations in the study area.

5.1. Modeling and Feature Selection

The DNN model constructed in this study comprised two types of data: Typhoon characteristics and surface meteorological data (see Section 2). When constructing the two respective ground-station wind-speed simulation models, the model input attributes excluded the station's own surface weather attributes (assuming that the stations were ungauged), as mentioned earlier, for the purpose of facilitating the evaluation of wind-speed values at any location in the study area. For example, when constructing the Taipei station wind-speed simulation model, this study used the meteorological data from the five neighboring stations at Keelung, Penjiayu, Tamsui, Banqiao, and Yilan to estimate the wind speed at Taipei station.

Based on the attributes of the data collected in this study, the number of model input attributes was discovered to potentially reach a total of as many as 46 (6 typhoon data attributes and 40 weather station attributes for the five stations). However, some attributes may not have exhibited a high degree of correlation with the objective attribute. Therefore, suitable attributes were required to be chosen before construction of the model. The strength of the correlations was assessed to select the model input variables. Typically, the correlations demonstrated a weak correlation, defined as r, in which the absolute value was less than 0.3 [51]; thus, this condition was set as a criterion (i.e., $|r| >= 0.3$) for selecting suitable attributes when constructing the models. On the basis of the analyzed correlations, attribute groups of $\{T_2, T_4, T_6, M_{1,1}, M_{1,6}, M_{1,8}, M_{2,1}, M_{2,6}, M_{3,1}, M_{3,6}, M_{3,8}, M_{4,1}, M_{4,6}, M_{6,1}, M_{6,6}, M_{6,8}\}$ were used as inputs for constructing the Taipei wind-simulation model, and attribute groups of $\{T_4, T_6, M_{2,6}, M_{3,6}, M_{3,8}, M_{4,1}, M_{4,6}, M_{4,8}, M_{5,1}, M_{5,6}, M_{5,8}, M_{6,1}, M_{6,6}, M_{6,8}\}$ were used for the Keelung wind-simulation model (these notations defined in Section 2). As a result, the attribute numbers of both models were 16 and 14, respectively.

5.2. Data Splitting and Model Construction

The training data (first 12 years, 2000–2011, involving 35 typhoons) were used to construct the models. Data from 2012–2017 were then used for validation and testing. The 10 validation typhoons (2012–2015) were used to evaluate the performance of the constructed models to confirm their suitability for generalization, and the two testing typhoons (2016–2017) were used to verify the selected models.

When constructing the DNN model, this study used a neural network structure that included an input layer, multiple hidden layers, and an output layer. The activity function of the hidden layers was the ReLU function, and the number of hidden-layer neurons was determined as the parameter setting based on the method recommended by [52]: (number of input layer neurons + number of output layer neuron − 1)/2. In this study, three parameters were required to be determined in the DNN model: Number of hidden layers, learning rate, and momentum correction coefficient. These three undetermined parameters were evaluated using a trial and error method, in which the initial momentum correction coefficient was assumed to be 0.2 and the number of hidden layers was assumed to be 5. A sensitivity analysis was then conducted to obtain the optimal learning rate. Because the respective ranges of the learning rate and momentum were between 0 and 1, this study divided each into 10 equal parts and respectively calculated the evaluation indicators for each interval value. The target value of the model output was the numerical wind-speed simulation value obtained by the WRF model for any positions (without wind speed observations).

The criterion RMSE was used to evaluate the error between the simulated and observed values here. Figure 7 presents the analysis results for parameter sensitivity when constructing the Taipei and Keelung station DNN models. Typically, a lower RMSE value correlates to a lower error. Thus, this study used the result with the lowest RMSE value as the preferred solution. As illustrated, the optimal learning rate, momentum, and number of hidden layers were respectively 0.1, 0.1, and 8 for Taipei station and 0.1, 0.1, and 2 for Keelung station.

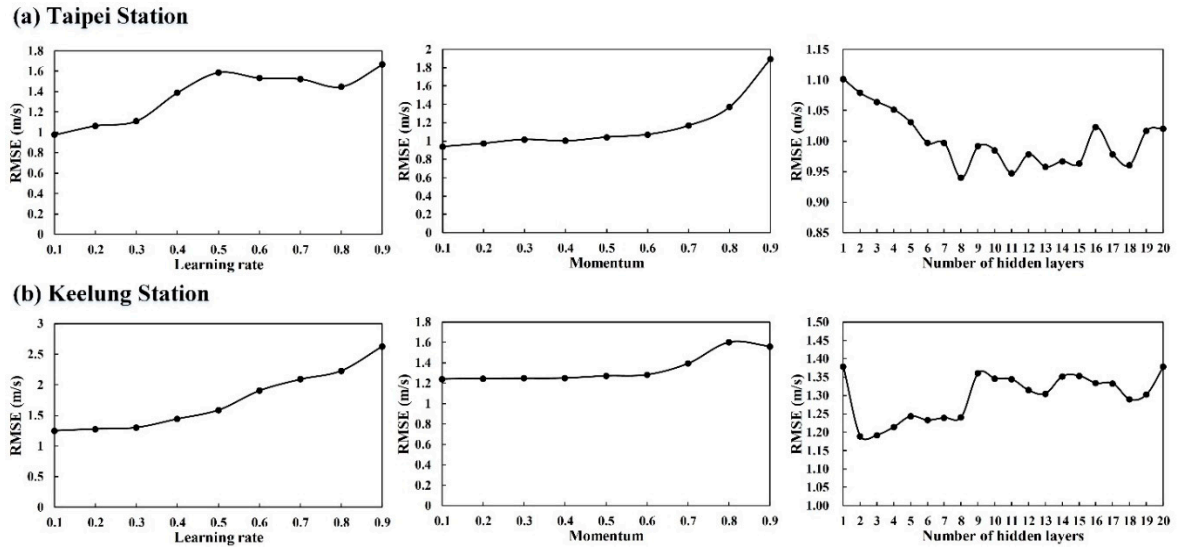

Figure 7. Sensitivity of DNN parameters on root mean squared error (RMSE): (**a**) Taipei station; (**b**) Keelung station.

5.3. Model Performance

Figure 8 presents the scatterplot diagram (using validation data set; blue solid line) for the DNN simulation values and WRF simulation values for the Taipei and Keelung stations. The analysis indicated that the r values of Taipei and Keelung stations' DNN vs. WRF were 0.8762 and 0.8405, respectively; thus, Taipei station had a greater r than Keelung station.

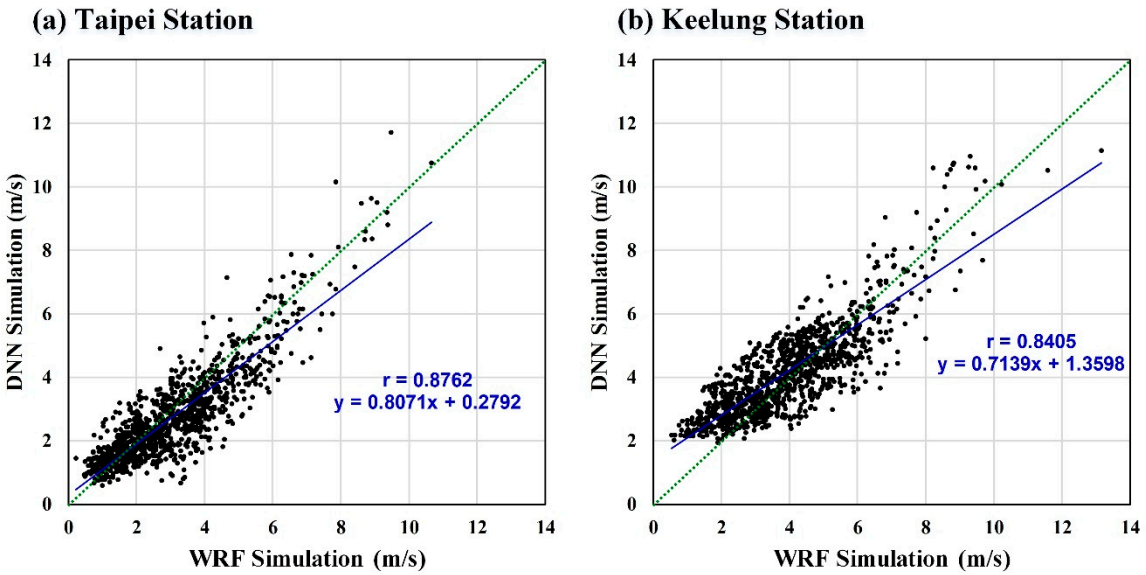

Figure 8. Scatterplots depicting the WRF simulations vs DNN simulations (using validation data set): (**a**) Taipei and (**b**) Keelung stations.

Here, the DNN model used the WRF simulation value as the target, because we assumed that the Taipei and Keelung stations are "ungauged stations." This study included the scatterplot for the DNN simulation values and WRF simulation values. The scatterplot in Figure 8 indicates the r values of Taipei and Keelung stations were 0.8762 and 0.8405, respectively. Furthermore, the results for error index performance indicated that the DNN model simulation results for Keelung station exhibited greater absolute and relative error than did those for Taipei station; for instance, the RMSE and rRMSE were respectively 1.373 m/s and 0.483 for Taipei station and 2.514 m/s and 0.500 for Keelung station.

5.4. Computing Efficiency

In the paper, we performed the model computing processes under the Intel Xeon E3-1240v6 3.70 GHz processor (Santa Clara, California, USA). The simulation time for each typhoon using WRF numerical model is approximately 3−15 h, and the computing time for building a DL-based DNN model measured approximately 30−80 s. By contrast, the DL-based DNN model demonstrates efficient.

6. Simulations of Testing Typhoons

Typhoons Megi (2016) and Nesat (2017) were selected for simulations in this section. Table 1 lists the characteristics of the two typhoons and the histories of the two typhoons are briefly described as follows:

Table 1. Typhoon characteristics of Megi in 2016 and Nesat in 2017.

Characteristics	Megi	Nesat
Duration of affecting periods	90 h	114 h
Average of pressure at typhoon center	958.9 hPa	972.4 hPa
Maximal typhoon radius of the winds over 15.5 m/s	225.6 km	159.5 km
Average moving speed of typhoon	18.3 km/h	16.6 km/h
Maximum wind speed of typhoon center	45 m/s	40 m/s

In 2016, Typhoon Megi gradually moved in a northwest–west direction after forming in the ocean near Guam (Figure 9a). On 1500 UTC 25 September 2016, the center of the typhoon was located to the southeast–east of Hualien in eastern Taiwan. The storm circle gradually approached the eastern half of Taiwan, and the center made landfall near Hualien city on 0600 UTC 27 September 2016. The typhoon center then passed through the CMR and changed course slightly to move in a southwestern direction before moving out to the sea near Wuqi, located in western Taiwan, at 1310 the same day. Megi caused 7 deaths and 625 injuries in Taiwan as well as US$83.3 million in agricultural damage.

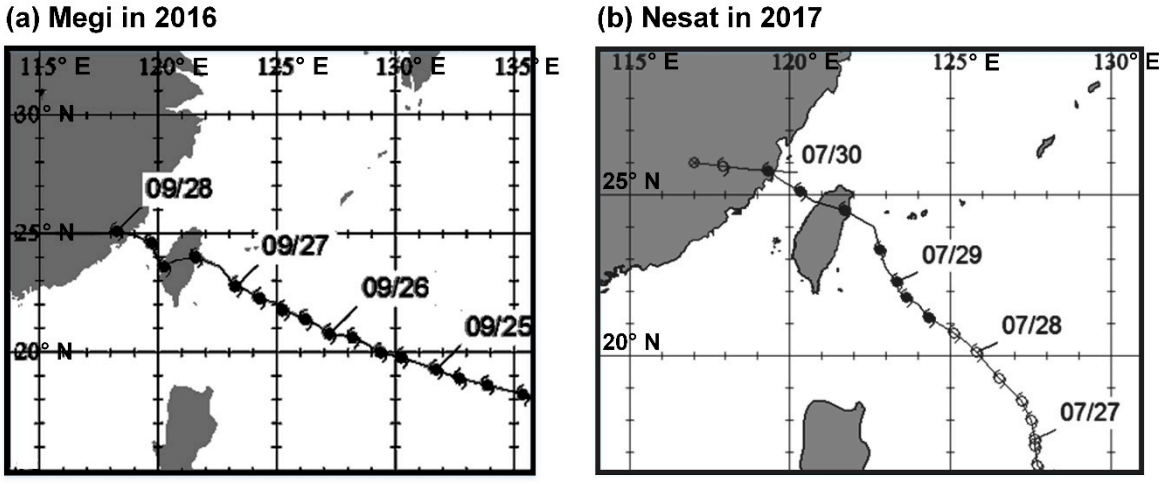

Figure 9. Historical typhoon tracks: (**a**) Megi in 2016 and (**b**) Nesat in 2017.

Typhoon Nesat originated in the southeastern seaboard in 2017 (Figure 9b). Nesat landed in Yilan County in eastern Taiwan on 1110 UTC 29 July 2017, and its movement accelerated after making landfall. Nesat left to sea on 1430 UTC 29 July 2017 from Miaoli County, located in western Taiwan. After entering mainland China, Nesat was greatly weakened. Nesat caused a total of 111 injuries in Taiwan, power loss in 586,145 households, and agricultural losses exceeding NT$6.7 million.

6.1. Simulation of Typhoon Megi

The first hour of the Megi typhoon time series (Figure 10) commenced on 0100 UTC 25 September 2016. Figure 10a illustrates that for observations (OBS), indicated by the gray-black solid line, Taipei station had three primary wind-speed periods. The first stage was before the typhoon center had landed (hours 1–45) with a steady wind speed between 2 and 8 m/s. The second stage commenced when the wind gradually strengthened after the typhoon center had landed (hour 46); during this stage, the wind speed increased substantially after the typhoon center had left to sea (hour 53), reaching its maximum value at hour 62 (13.1 m/s). After hour 69 (stage 3), the wind speed gradually weakened until it reached a breeze state. For Keelung station (Figure 10b), the wind speed was relatively low before the typhoon landed, after which it gradually strengthened and reached its maximum speed (18.2 m/s) when the typhoon was leaving to sea (hour 54).

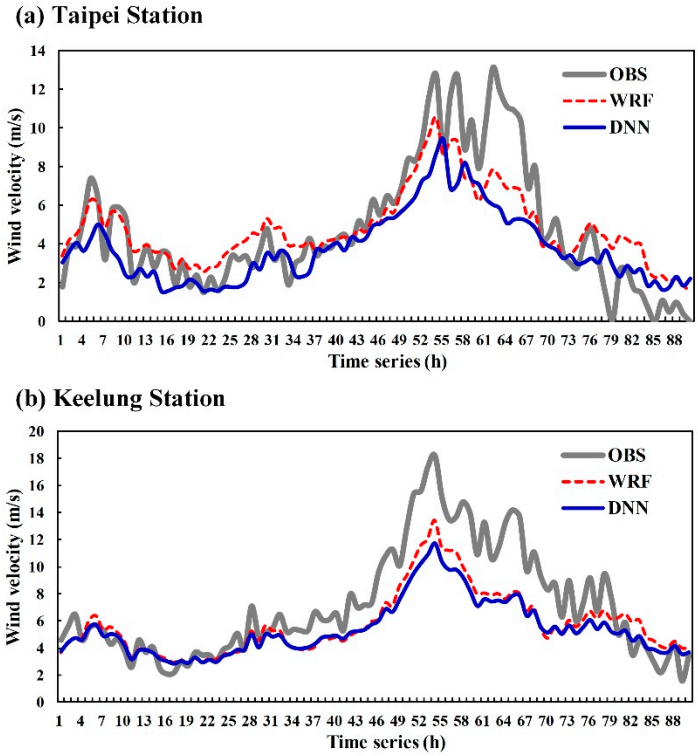

Figure 10. Observations and simulations of the wind velocity of Megi in 2016 at (**a**) Taipei and (**b**) Keelung stations.

Figure 10 presents the simulation results for the WRF and DNN models. In Figure 10a of Taipei station, the WRF model outcomes (red dotted line) were mostly consistent with observed values from hours 1 to 45 (before the typhoon landed), but compared with the values observed as the typhoon was strengthening (hour 46 to hour 68), they could be seen to have underestimated the wind speed. We can see the WRF model capture wind speed trends throughout the typhoon simulation. The overall simulated wind speed for the DNN model (solid blue line) was similar to that of the WRF model, but it exhibited an even greater degree of underestimation compared with the observed values. Furthermore, Figure 10b of Keelung station demonstrates that the observed values of the WRF mode were generally consistent from hours 1 to 33. However, when the typhoon was strengthening (hours 45–72), the model underestimated the wind speed in comparison with the observed values. For the DNN model, the overall wind-speed simulation was closer to the WRF model. However, compared with the observed values, the model still exhibited underestimation.

Figure 11 presents the MAE and RMSE evaluation indicator results for the WRF and DNN models of Typhoon Megi and demonstrates that the WRF model MAE and RMSE simulation-error indicator

results were superior to those of the DNN model. A comparison of the two stations again revealed that Keelung station exhibited greater absolute error compared with Taipei station.

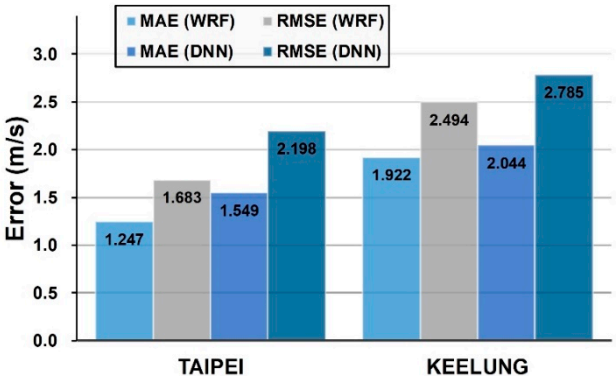

Figure 11. Performance levels of the Typhoon Megi in 2016.

6.2. Simulation of Typhoon Nesat

The first hour of Typhoon Nesat time series (Figure 12) commenced on 0100 UTC 26 July 2017. Figure 12a reveals that for observed values, Taipei station exhibited wind speeds between 0 and 6 m/s before the typhoon center had made landfall (hours 1–82), and the wind speed reached its maximum value (13.9 m/s) after the typhoon center's landfall (hours 83–87). The wind speed gradually weakened after the typhoon center left to sea (after hour 88). For Keelung station (Figure 12b), the wind speed gradually increased after the typhoon made landfall and reached a maximum value of 16.4 m/s. In general, Keelung station exhibited greater wind speed than did Taipei station.

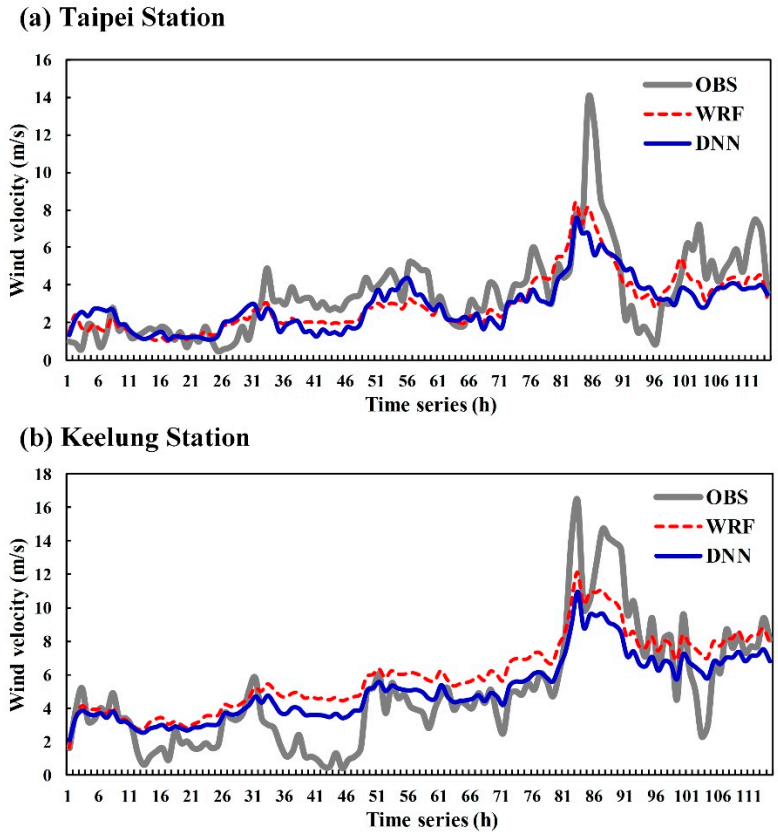

Figure 12. Observations and simulations of the wind velocity of Nesat in 2017 at (**a**) Taipei and (**b**) Keelung stations.

For the WRF and DNN model simulation results, Figure 12a reveals that the WRF model results for Taipei station were slightly lower than the observed value from hours 1 to 82 (before typhoon landing). When the typhoon strengthened (hours 83–87), the results underestimated the wind speed compared with the observed values. For the DNN model, the overall wind-speed simulation was generally consistent with that of the WRF model. Furthermore, Figure 12b demonstrates that the WRF model for Keelung station exhibited slightly higher wind speeds than the observed values from hours 1 to 82, but underestimated wind speeds when the typhoon was strengthening. The overall simulation produced slightly lower wind speeds for the DNN model than for the WRF model. Figure 13 presents the evaluation indicator results for the WRF and DNN models regarding the simulation of Typhoon Nesat and indicates that the MAE and RMSE simulation-error results at Taipei station of the WRF model were superior to those of the DNN model. At Keelung station, the MAE and RMSE simulation-error results of the DNN model were also superior to those of the WRF model, primarily because of the overestimation of the WRF model during periods with low wind speed, which led to the production of higher overall error in comparison with the DNN model.

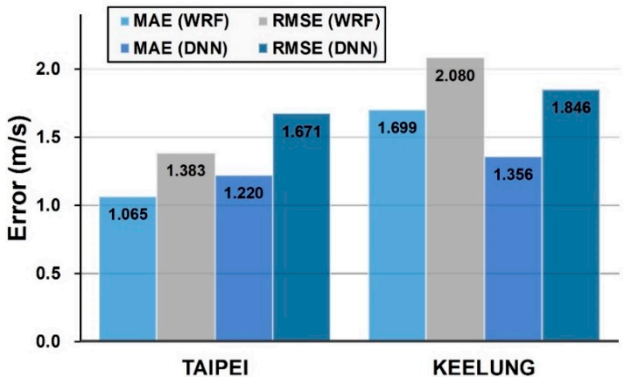

Figure 13. Performance levels of the Typhoon Nesat in 2017.

7. Conclusions

Typhoons in Taiwan bring not only torrents of rain but also the devastating, strong winds. Because of both the geographical location of Taiwan in the most common path for northwestern Pacific Ocean typhoons and its large variation in geographical altitude, strong winds throughout Taiwan are difficult to simulate. This study proposed a DL-based DNN model for simulating hourly wind speed during typhoons to establish highly reliable and efficient simulation techniques. The WRF model was employed as the numerical simulation-based model for precomputing solutions to determine the wind velocity at an arbitrary position where measures are absent. The DNN model was then used to construct the wind-simulation model by using the WRF wind outcomes as model targets. Consequently, this study verified the results of the DNN models according to the WRF simulations.

This study used Northern Taiwan as the study area for simulating wind speed. This study selected 47 typhoon events that had occurred between 2000 and 2017. Through the advantage of the ability of the WRF model to produce high-resolution simulations, this study simulated the local circulation of the study area with conditions closest to reality for each typhoon event to explore the influence of the terrain on typhoon circulation as well as the resulting spatial distribution and various features of local circulation. The DNN model was then used to ascertain the simulated values obtained from the WRF model for developing a wind-speed simulation model for any location in the study area. To verify the results of the model analysis, weather stations with records of wind speed observations were selected for use in a model comparison. Using Taipei and Keelung stations for comparison, this drew the following conclusions:

- The observed wind speeds for all past typhoons recorded at Keelung station ranged from 0 to 25 m/s. The observed wind speeds at Taipei station ranged from 0 to 15 m/s. This result is primarily

attributable to the effect of the terrain on typhoons; the effect on the wind speed at Taipei station, which is located in a basin area, was greater than the effect on Keelung station, which is located in a coastal area.

- In terms of WRF model performance, at both the Taipei and Keelung stations the WRF simulation values yielded an overestimation or underestimation when the wind speed was less than 9 m/s. However, the WRF simulation results produced an underestimation when the wind speed was greater than 9 m/s. The results for the two test typhoons, Megi and Nesat, indicated that the wind speed increased during the period between the typhoon landing and leaving land and was able to attain the maximum wind speed. Because the wind speed at this stage was approximately 9 m/s or greater, the WRF model still requires improvement with regard to simulating the period after typhoons land. Therefore, future studies can focus on the simulation process for this period of time. For example, studies can use sounding data from assimilation observation data or a combination of various physical parameters to improve the simulation results of wind speed.
- In terms of DNN model performance, both Keelung and Taipei stations underestimated the wind speed in comparison with the actual wind speed observations. Additionally, a comparison of the results of the two stations indicated that Keelung station exhibited a larger error and was more likely to underestimate the wind speed compared with Taipei station. This result is because the DNN model learns from the wind-speed simulation values of the WRF model. Therefore, when the simulation results of the WRF model underestimate the wind speed, the DNN model simulation results exhibit similar results (underestimation).
- In terms of overall model performance, both the WRF and DNN models tended to underestimate high wind speeds. However, both still could effectively demonstrate wind-speed trends. Thus, the conceptual model proposed in this study remains an effective method for simulating wind speed.

Future studies are likely to focus on enhancing the wind speed simulations at arbitrary points, for instance, replacing WRF simulation data with reanalysis data. For this research, we used the NCEP FNL reanalysis data as the input for simulating WRF model to obtain the wind speed simulations. Because the FNL data are on 1-degree by 1-degree resolution, the interpolation methods would be suggested to generate the wind speed simulations at arbitrary points. Moreover, in the research we built the DL-based DNN model to simulate wind speeds. However, this model did not address the spatial and temporal correlations of wind speeds among arbitrary points (or stations). Therefore, we suggest that the advanced DL-based neural networks, such as time-delay recurrent neural networks and convolutional neural networks, could be used for expanding the capability of the spatiotemporal sequences, because these approaches can be used to build a temporal system which can learn and memorize spatiotemporal sequences effectively.

Funding: The support for this study under Grant No. MOST106-2111-M-019-001 provided by the Ministry of Science and Technology, Taiwan is greatly appreciated.

Acknowledgments: The author acknowledges data provided by the Central Weather Bureau of Taiwan, and the Research Data Archive (RDA) at NCAR.

Conflicts of Interest: The authors declare no conflict of interest.

Appendix A

Typhoons Affecting Northern Taiwan over 2000–2017.

Table A1. Typhoons affecting the study area and their periods.

Year	Typhoon	Period (UTC)	Year	Typhoon	Period (UTC)
2000	Kai-Tak	6–10 Jul	2007	Sepat	16–19 Aug
2000	Bilis	21–23 Aug	2007	Wipha	17–19 Sep
2000	Xangsane	30 Oct–2 Nov	2007	Krosa	5–8 Oct
2001	Toraji	28–31 Jul	2008	Kalmaegi	16–19 Jul
2001	Nari	10–20 Sep	2008	Fung-Wong	27–29 Jul
2001	Lekima	24–29 Sep	2008	Sinlaku	10–16 Sep
2002	Nakri	9–11 Jul	2008	Jangmi	27–30 Sep
2002	Sinlaku	4–8 Sep	2009	Morakot	6–9 Aug
2004	Mindulle	29 Jun–3 Jul	2010	Namtheun	30–31 Aug
2004	Rananim	11–12 Aug	2010	Lionrock	31 Aug–2 Sep
2004	Aere	23–26 Aug	2010	Fanapi	18–20 Sep
2004	Haima	12–13 Sep	2012	Saola	30 Jul–3 Aug
2004	Nock-Ten	24–26 Oct	2012	Haikui	4–8 Aug
2004	Nanmadol	3–4 Dec	2013	Soulik	10–14 Jul
2005	Haitang	17–19 Jul	2013	Trami	16–22 Aug
2005	Matsa	3–6 Aug	2013	Kong-Rey	27–30 Aug
2005	Talim	31 Aug–1 Sep	2013	Fitow	2–7 Oct
2005	Khanun	10–11 Sep	2014	Matmo	21–23 Jul
2005	Longwang	1–2 Oct	2014	Fung-Wong	19–22 Sep
2006	Bilis	12–14 Jul	2015	Soudelor	6–9 Aug
2006	Kaemi	23–25 Jul	2015	Dujuan	25–29 Sep
2006	Bopha	8–9 Aug	2016	Megi	25–28 Sep
2006	Saomai	9–11 Aug	2017	Nesat	26–30 Jul
2006	Shanshan	14–16 Sep			

References

1. Wei, C.C. Conceptual weather environmental forecasting system for identifying potential failure of under-construction structures during typhoons. *J. Wind Eng. Ind. Aerodyn.* **2017**, *168*, 48–59. [CrossRef]
2. Al-Yahyai, S.; Charabi, Y.; Gastli, A. Review of the use of numerical weather prediction (NWP) models for wind energy assessment. *Renew. Sustain. Energy Rev.* **2010**, *14*, 3192–3198. [CrossRef]
3. Pielke, R.A.; Cotton, W.R.; Walko, R.L.; Tremback, C.J.; Lyons, W.A.; Grasso, L.D.M.; Nicholls, E.; Moran, M.D.; Wesley, D.A.; Lee, T.J.; et al. A comprehensive meteorological modeling system—RAMS. *Meteorol. Atmos. Phys.* **1992**, *49*, 69–91. [CrossRef]
4. Warner, T. *Numerical Weather and Climate Prediction*; Cambridge University Press: Cambridge, UK, 2010. [CrossRef]
5. Zhao, P.; Wang, J.; Xia, J.; Dai, Y.; Sheng, Y.; Yue, J. Performance evaluation and accuracy enhancement of a day-ahead wind power forecasting system in China. *Renew. Energy* **2012**, *43*, 234–241. [CrossRef]
6. Yang, M.J.; Ching, L. A modeling study of Typhoon Toraji (2001): Physical parameterization sensitivity and topographic effect. *Terr. Atmos. Ocean. Sci.* **2005**, *16*, 177–213. [CrossRef]
7. Davis, C.; Brown, B.; Bullock, R. Object-based verification of precipitation forecasts. Part I: Methodology and application to mesoscale rain areas. *Mon. Weather Rev.* **2006**, *134*, 1772–1784. [CrossRef]
8. Skamarock, W.C.; Klemp, J.B. A time-split nonhydrostatic atmospheric model for weather research and forecasting applications. *J. Comput. Phys.* **2008**, *227*, 3465–3485. [CrossRef]
9. Carvalho, D.; Rocha, A.; Gómez-Gesteira, M.; Santos, C. A sensitivity study of the WRF model in wind simulation for an area of high wind energy. *Environ. Model. Softw.* **2012**, *33*, 23–34. [CrossRef]
10. Skamarock, W.C.; Klemp, J.B.; Dudhia, J.; Gill, D.; Barker, D.; Duda, M.; Huang, X.Y.; Wang, W.; Powers, J.G. *A Description of the Advanced Research WRF Version 3*; NCAR Technical Note NCAR/TN-475+STR; NCAR: Boulder, CO, USA, 2008.
11. Huang, W.R.; Chang, Y.H.; Hsu, H.H.; Cheng, C.T.; Tu, C.Y. Dynamical downscaling simulation and future projection of summer rainfall in Taiwan: Contributions from different types of rain events. *J. Geophys. Res. Atmos.* **2016**, *121*, 13973–13988. [CrossRef]

12. Di, Z.; Gong, W.; Gan, Y.; Shen, C.; Duan, Q. Combinatorial optimization for WRF physical parameterization schemes: A case study of three-day typhoon simulations over the Northwest Pacific Ocean. *Atmosphere* **2019**, *10*, 233. [CrossRef]
13. Ming, F.C.; Jolivet, S.; Liou, Y.A.; Jégou, F.; Mekies, D.; Hong, J.S. Elliptical structures of gravity waves produced by Typhoon Soudelor in 2015 near Taiwan. *Atmosphere* **2019**, *10*, 260. [CrossRef]
14. Mylonas, M.P.; Douvis, K.C.; Polychroni, I.D.; Politi, N.; Nastos, P.T. Analysis of a Mediterranean tropical-like cyclone: Sensitivity to WRF parameterizations and horizontal resolution. *Atmosphere* **2019**, *10*, 425. [CrossRef]
15. Ricchi, A.; Miglietta, M.M.; Barbariol, F.; Benetazzo, A.; Bergamasco, A.; Bonaldo, D.; Cassardo, C.; Falcieri, F.M.; Modugno, G.; Russo, A.; et al. Sensitivity of a Mediterranean tropical-like cyclone to different model configurations and coupling strategies. *Atmosphere* **2017**, *8*, 92. [CrossRef]
16. Wei, C.C. Wavelet support vector machines for forecasting precipitation in tropical cyclones: Comparisons with GSVM, regression, and MM5. *Weather Forecast.* **2012**, *27*, 438–450. [CrossRef]
17. Tao, W.K.; Shi, J.J.; Lin, P.L.; Chen, J.; Lang, S.; Chang, M.Y.; Yang, M.J.; Wu, C.C.; Peters-Lidard, C.; Sui, C.H.; et al. High-resolution numerical simulation of the extreme rainfall associated with typhoon Morakot. Part I: Comparing the impact of microphysics and PBL parameterizations with observations. *Terr. Atmos. Ocean. Sci.* **2011**, *22*, 673–696. [CrossRef]
18. Xu, X.; Lu, C.; Xu, H.; Chen, L. A possible mechanism responsible for exceptional rainfall over Taiwan from Typhoon Morakot. *Atmos. Sci. Lett.* **2011**, *12*, 294–299. [CrossRef]
19. Hsiao, L.F.; Yang, M.J.; Lee, C.S.; Kuo, H.C.; Shih, D.S.; Tsai, C.C.; Wang, C.J.; Chang, L.Y.; Chen, D.Y.C.; Feng, L.; et al. Ensemble forecasting of typhoon rainfall and floods over a mountainous watershed in Taiwan. *J. Hydrol.* **2013**, *506*, 55–68. [CrossRef]
20. Wu, Z.; Jiang, C.; Deng, B.; Chen, J.; Liu, X. Sensitivity of WRF simulated typhoon track and intensity over the South China Sea to horizontal and vertical resolutions. *Acta Oceanol. Sin.* **2019**, *38*, 74–83. [CrossRef]
21. Smola, A.; Vishwanathan, S.V.N. *Introduction to Machine Learning*; Cambridge University Press: Cambridge, UK, 2008.
22. Wei, C.C. Meta-heuristic Bayesian networks retrieval combined polarization corrected temperature and scattering index for precipitations. *Neurocomputing* **2014**, *136*, 71–81. [CrossRef]
23. Wei, C.C. Comparing lazy and eager learning models for water level forecasting in river-reservoir basins of inundation regions. *Environ. Model. Softw.* **2015**, *63*, 137–155. [CrossRef]
24. Currie, J.J.; Goulet, P.J.; Ratsimandresey, A.W. Wind conditions in a Fjordlike Bay and predictions of wind speed using neighboring stations employing neural network models. *J. Appl. Meteorol. Climatol.* **2014**, *53*, 1525–1537. [CrossRef]
25. Etienne, C.; Lehmann, A.; Goyette, S.; Lopez-Moreno, J.; Beniston, M. Spatial predictions of extreme wind speeds over Switzerland using generalized additive models. *J. Appl. Meteorol. Climatol.* **2010**, *49*, 1956–1970. [CrossRef]
26. Kozar, M.E.; Misra, V.; Powell, M.D. Hindcasts of integrated kinetic energy in Atlantic tropical cyclones: A neural network prediction scheme. *Mon. Weather Rev.* **2016**, *144*, 4591–4603. [CrossRef]
27. Liu, H.; Tian, H.; Li, Y. An EMD-recursive ARIMA method to predict wind speed for railway strong wind warning system. *J. Wind Eng. Ind. Aerodyn.* **2015**, *141*, 27–38. [CrossRef]
28. Wei, C.C. Surface wind nowcasting in the Penghu Islands based on classified typhoon tracks and the effects of the Central Mountain Range of Taiwan. *Weather Forecast.* **2014**, *29*, 1425–1450. [CrossRef]
29. Wei, C.C. Examining El Niño–Southern Oscillation effects in the subtropical zone to forecast long-distance total rainfall from typhoons: A case study in Taiwan. *J. Atmos. Ocean. Technol.* **2017**, *34*, 2141–2161. [CrossRef]
30. Yang, J.; Astitha, M.; Anagnostou, E.N.; Hartman, B.M. Using a Bayesian regression approach on dual-model windstorm simulations to improve wind speed prediction. *J. Appl. Meteorol. Climatol.* **2017**, *56*, 1155–1174. [CrossRef]
31. Li, L.; Xiao, Y.; Kareem, A.; Song, L.; Qin, P. Modeling typhoon wind power spectra near sea surface based on measurements in the South China sea. *J. Wind Eng. Ind. Aerodyn.* **2012**, *104–106*, 565–576. [CrossRef]
32. Wei, C.C. Forecasting surface wind speeds over offshore islands near Taiwan during tropical cyclones: Comparisons of data-driven algorithms and parametric wind representations. *J. Geophys. Res. Atmos.* **2015**, *120*, 1826–1847. [CrossRef]
33. Hu, Q.; Zhang, R.; Zhou, Y. Transfer learning for short-term wind speed prediction with deep neural networks. *Renew. Energy* **2016**, *85*, 83–95. [CrossRef]

34. Hinton, G.E.; Osindero, S.; Teh, Y.W. A fast learning algorithm for deep belief nets. *Neural Comput.* **2014**, *18*, 1527–1554. [CrossRef] [PubMed]
35. Krinitskiy, M.; Verezemskaya, P.; Grashchenkov, K.; Tilinina, N.; Gulev, S.; Lazzara, M. Deep convolutional neural networks capabilities for binary classification of polar mesocyclones in satellite mosaics. *Atmosphere* **2018**, *9*, 426. [CrossRef]
36. Wei, C.C.; Peng, P.C.; Tsai, C.H.; Huang, C.L. Regional forecasting of wind speeds during typhoon landfall in Taiwan: A case study of westward-moving typhoons. *Atmosphere* **2018**, *9*, 141. [CrossRef]
37. Tsai, C.C.; Wei, C.C.; Hou, T.H.; Hsu, T.W. Artificial neural network for forecasting wave heights along a ship's route during hurricanes. *J. Waterw. Port Coast. Ocean Eng.* **2018**, *144*, 04017042. [CrossRef]
38. Wang, W.; Bruyère, C.; Duda, M.; Dudhia, J.; Gill, D.; Kavulich, M.; Keene, K.; Lin, H.-C.; Michalakes, J.; Rizvi, S.; et al. *WRF Version 3 Modeling System User's Guide*; Mesoscale & Microscale Meteorology Division, National Center for Atmospheric Research: Boulder, CO, USA, 2016.
39. Du, J.; Xu, Y. Hierarchical deep neural network for multivariate regression. *Pattern Recognit.* **2017**, *63*, 149–157. [CrossRef]
40. Cheng, J.; Chen, X.; Metallinou, A. Deep neural network acoustic models for spoken assessment applications. *Speech Commun.* **2015**, *73*, 14–27. [CrossRef]
41. Nair, V.; Hinton, G. Rectified linear units improve restricted Boltzmann machines. In Proceedings of the 27th International Conference on Machine Learning, Haifa, Israel, 21–24 June 2010; pp. 807–814.
42. Sze, V.; Chen, Y.H.; Yang, T.J.; Emer, J.S. Efficient processing of deep neural networks: A tutorial and survey. *Proc. IEEE* **2017**, *105*, 2295–2329. [CrossRef]
43. Yeh, T.C.; Chen, S.H.; Hong, J.S. *The Forecast Technique Development Studies on the Typhoon Track, Rainfall and Winds Forecast over Taiwan Area: A Study on the Implementation of WRF Typhoon Forecasting Component in the Operational Environment of CWB*; Funded by Ministry of Science and Technology of Taiwan, No. NSC96-2625-Z-052-003; MOST: Taipei, Taiwan, 2008. (In Chinese)
44. Yeh, T.C.; Terng, C.T.; Lee, C.S.; Yang, M.J. *The Forecast Technique Development Studies on the Typhoon Track, Rainfall and Winds Forecast over Taiwan Area: A Study on the Implementation of WRF Typhoon Forecasting Component in the Operational Environment of CWB (II)*; Funded by Ministry of Science and Technology of Taiwan, No. NSC97-2625-M-052-002; MOST: Taipei, Taiwan, 2009. (In Chinese)
45. Yeh, T.C.; Terng, C.T.; Lee, C.S.; Yang, M.J. *The Forecast Technique Development Studies on the Typhoon Track, Rainfall and Winds Forecast over Taiwan Area: A Study on the Implementation of WRF Typhoon Forecasting Component in the Operational Environment of CWB (III)*; Funded by Ministry of Science and Technology of Taiwan, No. NSC-98-2625-M-052-008; MOST: Taipei, Taiwan, 2010. (In Chinese)
46. Hong, S.Y.; Pan, H.L. Nonlocal boundary layer vertical diffusion in a medium-range forecast model. *Mon. Weather Rev.* **1996**, *124*, 2322–2339. [CrossRef]
47. Hong, S.Y.; Dudhia, J.; Chen, S.H. A revised approach to ice microphysical processes for the bulk parameterization of clouds and precipitation. *Mon. Weather Rev.* **2004**, *132*, 103–120. [CrossRef]
48. Kain, J.S.; Fritsch, J.M. A one-dimensional entraining/detraining plume model and its application in convective parameterization. *J. Atmos. Sci.* **1990**, *47*, 2784–2802. [CrossRef]
49. Kain, J.S.; Fritsch, J.M. *Convective Parameterization for Mesoscale Models: The Kain-Fritsch Scheme*; The Representation of Cumulus Convection in Numerical Models; Meteorological Monographs, No. 24; American Meteor Society: Geneseo, NY, USA, 1993; pp. 165–170.
50. Mlawer, E.J.; Clough, S.A. On the extension of RRTM to the shortwave region. In Proceedings of the Sixth Atmospheric Measurement (ARM) Science Team Meeting, CONF-9603149, San Antonio, TX, USA, 4–7 March 1996; U.S. Department of Energy: Washington, DC, USA, 1997; pp. 223–226.
51. Taylor, R. Interpretation of the correlation coefficient: A basic review. *J. Diagn. Med. Sonogr.* **1990**, *1*, 35–39. [CrossRef]
52. Trenn, S. Multilayer perceptrons: Approximation order and necessary number of hidden units. *IEEE Trans. Neural Netw.* **2008**, *19*, 836–844. [CrossRef] [PubMed]